No evidence of millimetre excess emission in the Crab Nebula

Juan Francisco Macias-Perez, F. Mayet, F.X. Desert, J. Aumont

Astronomy & Astrophysics manuscript no. ArcheoCrab.hyper26397
February 4, 2008

No evidence of millimetre excess emission in the Crab Nebula

J. F. Macías-Pérez [1], F. Mayet[1], F.-X. Désert[2], and J. Aumont[1] ⋆

[1] LPSC, Université Joseph Fourier Grenoble 1, CNRS/IN2P3, Institut National Polytechnique de Grenoble, 53, av. des Martyrs, 38026 Grenoble, France
[2] Laboratoire d'Astrophysique, Obs. de Grenoble, BP 53, 38041 Grenoble Cedex 9, France

February 4, 2008

ABSTRACT

Aims. We present a comprehensive study of the Crab Nebula spectral energy distribution (SED) over more than 6 decades in frequency ranging from 1 to 10^6 GHz. We focus on the millimetre regime where an excess of flux has been claimed. For this purpose we use new radio and submillimetre data from the WMAP satellite between 23 and 94 GHz and from the Archeops balloon experiment between 143 and 545 GHz, and a compendium of already published Crab Nebula observations.

Methods. The Crab SED has been compared to models including three main components : synchrotron which is responsible for the emission at low and at high frequencies, dust which explains the excess of flux observed by the IRAS satellite and an extra component to account for a possible millimetre excess.

Results. For this extra component we have considered both a low–temperature dust and a low–energy cutoff synchrotron. In the case of extra dust component the best fit model requires extremely low dust temperatures of 5-6 K and therefore a large dust mass of ∼110-230 $M_\odot$, making the model fully unrealistic. In any case the extra dust component does not significantly improve the fit to the data in the millimetric regime from 100 to 1000 GHz. For the case of an extra synchrotron component we find that the spectral index of the energy distribution and the cutoff frequency are not constrained by the model. More importantly the best-fit to the data has larger residuals in the millimetric regime that when assuming no extra component.

Conclusions. The currently available data in the unpolarised emission of the Crab Nebula show no evidence of millimetric excess with respect to the known synchrotron emission. This is important for the Planck satellite mission which will use the Crab nebula for polarisation cross-checks in the range 30 to 857 GHz.

Key words. ISM: individual objects: Crab Nebula - calibration - cosmic microwave background

1. Introduction

As the strongest source of synchrotron radiation in our galaxy, the pulsar-powered Crab nebula (*Taurus A*) is a well studied astrophysical object and it is therefore used for calibration purpose. This will be the case for the Planck satellite mission which will use the Crab Nebula for polarisation cross-checks in the frequency range from 30 to 857 GHz. A good understanding of the SED of the source as well as of the total intensity flux within the Planck beam will be required for an accurate determination of the angle of polarisation of the detectors and of a possible cross polarisation effect between detector as they limit the accuracy to which the CMB polarised angular power spectra will be measured.

The emission spectrum of the A.D. 1054 supernova remnant has been the subject of a host of investigations over several decades in frequency. The radio spectrum is known to exhibit a synchrotron power law with a spectral index $\beta \simeq -0.299 \pm 0.009$ (Baars *et al.* (1977)). This continuum from radio synchrotron seems to be fading with a rate $\alpha = (-0.167 \pm 0.015)\%\mathrm{yr}^{-1}$ (Aller & Reynolds (1985)). At higher frequency, above 10^4 GHz, the observation are also consistent with synchrotron emission with a power-law of spectral index −0.73 (Veron-Cetty & Woltjer (1993)).
The data from IRAS satellite (Marsden *et al.* (1984)) have been reanalyzed by Strom & Greidanus (1992) revealing a significant excess of emission over the low frequency synchrotron spectrum, well explained by a single dust component at a temperature T ∼ 46 K, thus requiring a 0.02 $M_\odot$ dust mass. Using MPifrR bolometer arrays at the IRAM 30 m telescope, Bandiera *et al.* (2002) gave the first evidence for a new component at milllimetre wavelengths. They have shown that this 1.3 mm excess flux cannot be interpreted as emission from a dust component whereas the data may be consistent with a low energy cutoff in the energy distribution of the emitting particles. However this excess of flux is based on a unique measurement at 1.3 mm.

Send offprint requests to: macias@lpsc.in2p3.fr
⋆ Currently at CESR, 9 Avenue du Colonel Roche, 31028 Toulouse cedex 4, France

In this paper, we use recent observations of the Crab Nebula by the WMAP satellite at 23, 33, 41, 61 and 94 GHz (Page *et al.* 2006) and by the Archeops balloon experiment at 143, 217, 345 and 545 GHz (Macías-Pérez *et al.* (2007), Desert *et al.* (2008)). These data in addition to already published data are used to study the Crab Nebula SED in order to assess the validity of the millimetre excess proposed by Bandiera *et al.* (2002). The paper is organized as follows. Sect. 2 presents the SED of the Crab Nebula from 1 to 10^6 GHz and compares it to a model including the synchrotron and dust well known components. In Sect. 3 we perform a coherent analysis of the Crab SED over the full frequency range adding an extra component to the previous model to account for the possible millimetre excess. Summary and conclusions are given in Sect. 4.

2. SED of the Crab Nebula

We present in this section a coherent analysis of the Crab SED in the range 1 to 10^6 GHz based on a compendium of observations[1] shown in Table 1. Notice that to be able to directly compare to the Archeops and WMAP data, we have chosen only those data sets for which integrated fluxes over the full extension of the Crab Nebula are available.

2.1. Low-frequency synchrotron emission

An accurate determination of the low-frequency synchrotron component is necessary to assess the synchrotron contribution at mm frequencies. Any inter-comparison of low-frequency radio observations of the Crab nebula must take into account its well-known secular decrease. In particular Aller & Reynolds (1985) have estimated a secular decrease in the flux density at a rate $\alpha = (-0.167 \pm 0.015)\ \%yr^{-1}$ from observations at 8 GHz over the period 1968 to 1984. This result is in good agreement with other studies at lower frequencies: for example $\alpha = (-0.18 \pm 0.1)\ \%yr^{-1}$ over the period 1977 to 2000 at 927 MHz by Vinyajkin (2005).

All these measurements are in fair agreement with theoretical evaluations of the evolution of pulsar driven supernova remnants by Reynolds & Chevalier (1984) which predicts α ranging from -0.16% to $-0.4\%yr^{-1}$.
For this paper the value $\alpha = -0.167\ \%yr^{-1}$ is chosen for the fading of the Crab Nebula and all data are converted to a common observation date, 01/01/2003. In figure 1 we trace the flux of the Crab Nebula as a function of frequency for the fading corrected low-frequency data in table 1 ranging from 1 to 143 GHz. We observe a large decrease of flux with increasing frequency which can be represented by a power law of the form $A_1 \left(\frac{\nu}{1\mathrm{GHz}}\right)^{\beta_1}$. By χ^2 minimization, we obtain for the low-frequency data up to 100 GHz

$$\beta_1 = -0.324 \pm 0.006 \text{ and } A_1 = (1005 \pm 18)\ Jy$$

with $\chi^2/\mathrm{N_{dof}} = 1.03$ shown as a red solid line on Fig 1. This result is not in agreement with the "canonical" value $\beta \simeq -0.299 \pm 0.009$ from Baars *et al.* (1977) [2]. However when

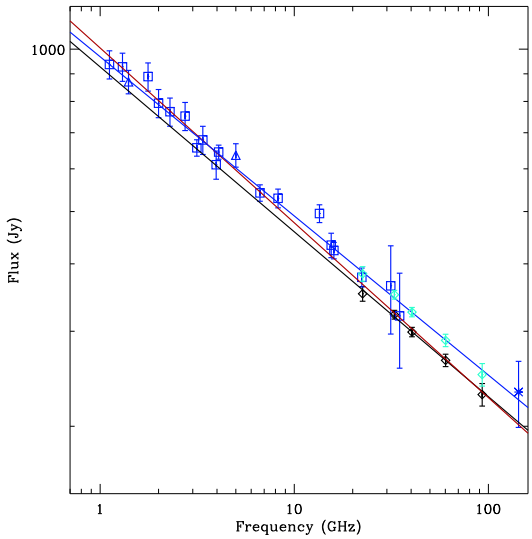

Fig. 1. SED of the Crab Nebula from 1 to 100 GHz. The red line corresponds to a global power-law best-fit of the data as described in the test. The blue line corresponds to the power-law best-fit to the data excluding the WMAP data (black diamonds). The black line corresponds to the power-law best-fit to the data using only the WMAP data. The light blue diamonds are the WMAP data (black diamonds) increased by 8 %.

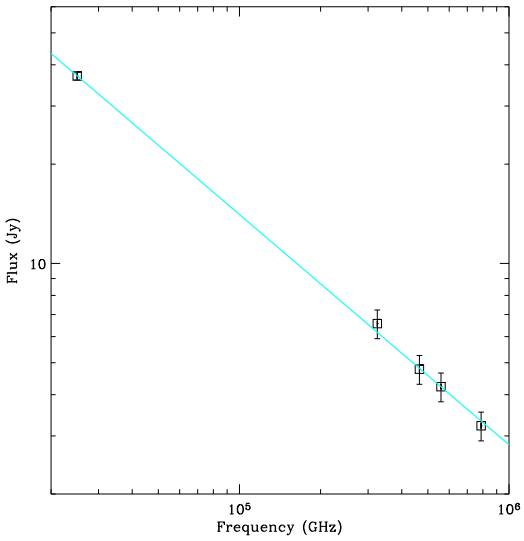

Fig. 2. High frequency SED of the Crab Nebula. Data samples are represented in black. The best-fit power law model to the data is overplotted (see text for details).

[1] Green *et al.* (2004) data at 850 μm was not used as no accurate estimate of the total flux and its error bar are given. The value of the flux proposed by the authors is $\sim$ 190 Jy is in agreement with the Archeops data at 850 μm with a flux 186 ± 33Jy.

[2] Kovalenko *et al.* (1994) obtained $\beta_1 = (-0.27 \pm 0.04)$

ν (GHz)	S_ν (Jy)	ΔS_ν (Jy)	Central Epoch	Reference
1.117	990.0	59.4	1969.9	Vinogradova *et al.* (1971)
1.304	980.0	58.8	1969.9	Vinogradova *et al.* (1971)
1.4	930.0	46.5	1963	Kellermann *et al.* (1969)
1.765	940.0	56.4	1969.9	Vinogradova *et al.* (1971)
2.0	840.0	50.4	1969.3	Dmitrenko *et al.* (1970)
2.29	810.0	48.6	1969.3	Dmitrenko *et al.* (1970)
2.74	795.0	47.7	1969.3	Dmitrenko *et al.* (1970)
3.15	700.0	24.5	1964.4	Medd (1972)
3.38	718.0	43.1	1969.3	Dmitrenko *et al.* (1970)
3.96	646.0	38.8	1969.3	Dmitrenko *et al.* (1970)
4.08	687.0	20.6	1964.8	Penzias & Wilson (1965)
5.0	680	34	1963	Kellermann *et al.* (1969)
6.66	577.2	20.2	1965.	Medd (1972)
8.25	563.0	22.5	1965.9	Allen & Barrett (1967)
13.49	524.0	19.9	1969.9	Medd (1972)
15.5	461	24	1965.9	Allen & Barrett (1967)
16.0	447.0	15.6	1970.6	Wrixon *et al.* (1972)
22.285	397	16.0	1973.1	Janssen *et al.* (1974)
22.5	401	11	2003	Page *et al.* 2006
31.41	387	72	1966.7	Hobbs *et al.* (1968)
32.8	367	6	2003	Page *et al.* 2006
34.9	340	68	1967.3	Kalaghan & Wulfsberg (1967)
40.4	340.9	6.0	2003	Page *et al.* 2006
60.2	302.1	7.0	2003	Page *et al.* 2006
92.9	261.1	11.0	2003	Page *et al.* 2006
111,1	290	35	1973.5	Zabolotnyi *et al.* (1976)
143	231.4	32.4	2002	Desert *et al.* (2008)
217	181.9	38.2	2002	Desert *et al.* (2008)
230	260	52	2000	Bandiera *et al.* (2002)
250	204	32	1985.3	Mezger *et al.* (1986)
300	194.0	19.4	1983	Chini *et al.* (1984)
300	131	42	1978.75	Wright *et al.* (1979)
300	300	80	1976.0	Werner *et al.* (1977)
353	185.9	33.6	2002	Desert *et al.* (2008)
545	236.6	68.4	2002	Desert *et al.* (2008)
750	158	63	1978.75	Wright *et al.* (1979)
1000	135	41	1978.75	Wright *et al.* (1979)
3000	184	13	1983.5	Strom & Greidanus (1992)
5000	210	8	1983.5	Strom & Greidanus (1992)
12×10^3	67	4	1983.5	Strom & Greidanus (1992)
25×10^3	37	1	1983.5	Strom & Greidanus (1992)
3.246×10^5	6.57	0.66	1989	Veron-Cetty & Woltjer (1993)
4.651×10^5	4.78	0.48	1989	Veron-Cetty & Woltjer (1993)
5.593×10^5	4.23	0.42	1989	Veron-Cetty & Woltjer (1993)
7.878×10^5	3.22	0.32	1989	Veron-Cetty & Woltjer (1993)

Table 1. Compendium of Crab Nebula observations from 1 to 10^6 GHz. Fluxes (S_ν) are presented in Jy. For Veron-Cetty & Woltjer (1993) and Chini *et al.* (1984) a conservative 10% error has been chosen to account for extrapolation errors. The central epoch of observation is also indicated. This is used for the evaluation of the fading effect of the low frequency synchrotron component, up to $\sim$ 100 GHz.

we exclude the WMAP data (black data points), we find

$$\beta_1 = -0.294 \pm 0.012 \text{ and } A_1 = (968 \pm 22) \text{ Jy}$$

with $\chi^2/N_{dof} = 0.78$ (blue solid line on Fig.1) in good agreement with the canonical value. Furthermore, using only the WMAP data we obtain

$$\beta_1 = -0.305 \pm 0.03 \text{ and } A_1 = (927 \pm 107)\ Jy$$

with $\chi^2/N_{dof} = 0.20$ (solid black line on Fig 1) for which the power law exponent, β_1, is in good agreement with the canonical value and the amplitude A_1 is $\sim$ 8 % lower.

The incompatibility of the above results can be explained either by inter-calibration errors of $\sim$ 8 % or by an evolution of the synchrotron SED towards a harder spectrum or by a dramatic change of the fading with time. The latter seems to be quite unlikely and no other indication of evolution

on the synchrotron spectrum at those frequencies has been claimed yet. To illustrate a possible intercalibration error we also trace on Fig 1 the WMAP data increased by 8 % (light blue diamonds) to make them compatible with the rest of the low-frequency data.

However, the data we use does not clearly favor any of the above options and a more detailed study of this problem is out of the scope of this paper. Indeed, we are only interested in quantifying a possible excess of flux at millimetric wavelengths with respect to the low frequency synchrotron emission. Therefore, being conservatives, hereafter and for all the analyses performed we will use three different data sets: the first one containing the full low frequency data set except WMAP (data set A), the second one containing only the WMAP data at low frequency (data set B) and the last one considering the full data set at low frequency (data set C). Table 2 summarizes the parameters for the best-fit model to the three data sets for the low-frequency synchrotron spectrum.

Data Set	χ^2/N_{dof}	$A_1(Jy)$	β_1
All except WMAP: A	0.78	968 ± 22	-0.294 ± 0.012
Only WMAP: B	0.20	927 ± 107	-0.305 ± 0.03
All: C	1.03	1005 ± 18	-0.324 ± 0.006

Table 2. χ^2/N_{dof} value and parameters for the best-fit model to the data for the low-frequency synchrotron spectrum. See text for detail description of the A, B and C data sets.

2.2. High frequency synchrotron and dust emission

The Crab synchrotron emission described above evolves at higher frequencies, around 10^4 GHz, towards a much harder SED with a spectral index of ~ -0.73 (see for example Veron-Cetty & Woltjer (1993)). To accurately estimate the synchrotron emission properties at high frequency we have fitted the data from 10^4 to 10^6 GHz presented in table 1 to a power law of the form $A_2\nu^{\beta_2}$. By χ^2 minimization, we found the data to be well fitted, $\chi^2/\mathrm{N_{dof}} = 0.155$, by a power law of parameters

$$\beta_2 = (-0.698 \pm 0.018) \text{ and } \mathrm{A_2} = (43.5 \pm 8.8) \times 10^3 \,\mathrm{Jy}$$

Figure 2 represents the high-frequency data in black and the best-fit power law model in red.

Finally, the infrared satellite observatory IRAS has revealed significant excess emission above this synchrotron contribution around 50 μm (Marsden *et al.* (1984)). As shown by Strom & Greidanus (1992) this can be explained, after careful removing of the synchrotron component, by a single dust component described by a modified black body of emissivity $\beta = 2$ at T= 46 ± 3 K, requiring a dust mass of 0.02 $\mathrm{M_\odot}$.

2.3. Millimetric excess

To evaluate a possible millimetric excess of flux in the range 100 to 1000 GHz we assume the above canonical modeling of the Crab nebula SED: a synchrotron component with a spectral index break at high frequency and a dust component at infrared wavelengths. We can thus reconstruct the Crab nebula emission at the millimetric frequencies and compare it to the data in table 1. For the low-frequency synchrotron emission we consider the best-fit for the three data sets A (all data but except WMAP), B (only WMAP at low frequencies) and C (all data). From left to right Fig 3 shows the residuals to the canonical model from 10 to 2×10^4 GHz for data sets A, B and C, respectively. For clarity, the residuals for the Archeops data are represented in red on the figure. We observe that there is no significant excess of power in the millimetric regime from 100 to 1000 GHz except for the 545 GHz Archeops data sample which presents only a 1.5 sigma excess. Indeed, the χ^2/N_{dof} for the null hypothesis are 0.68, 1.15 and 1.32 for the data sets A, B and C, respectively.

3. Refined modeling

In the previous section we have proved that the millimetric data in table 1, from 100 to 1000 GHz, are compatible with the canonical model assuming single synchrotron and dust components. However, it is interesting to check if an extra component may improve significantly the fit to the data. Following Bandiera *et al.* (2002) we consider either an extra low-temperature dust emission or an extra synchrotron component. Thus, the three component model is defined as follows

1. Canonical synchrotron that is described by four parameters: spectral index and amplitude for the low and high frequency emission. At high frequency we consider both the amplitude and the spectral index fixed and set them to the values obtained in Sect. 2.2. At low frequency we fix the spectral index to the value obtained in Sect. 2.1 and the amplitude, A_S, is fitted. We also assume a constant fading of $\alpha = -0.167\ \%yr^{-1}$ as before.
2. Canonical dust (following Strom & Greidanus (1992)) described by a modified black body with three free parameters, A_D, T_D and β_D that represent the amplitude, temperature and spectral index respectively.
3. One of the extra components as described below.

3.1. Extra low-temperature dust emission

In Sect. 2.3 we concluded that at 545 GHz the difference between the standard model and the data is at its maximum. In the case of an extra dust component this implies very low temperature dust in the range from 4 to 10 K. To model this component we assume a modified black body spectrum with three free parameters A_{LTD}, T_{LTD} and β_{LTD} that represent the amplitude, temperature and spectral index respectively. The best-fit model to the data is found by χ^2 minimization on the full frequency range from 1 to 10^6 GHz. As above we have performed our analysis on data sets A, B and C.

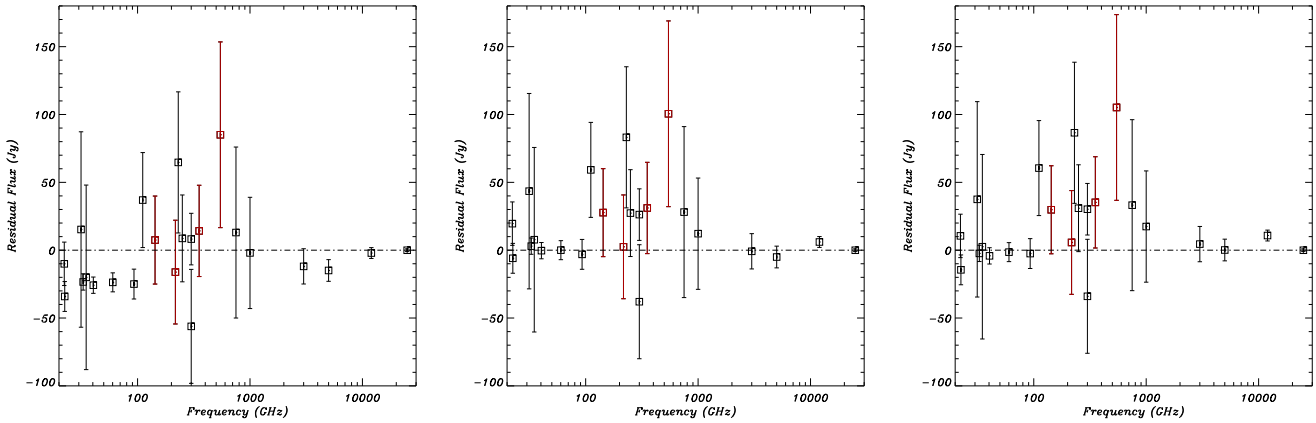

Fig. 3. From left to right plots represent in the frequency range from 10 to 2000 GHz the residuals to the standard model of the Crab nebula emission assuming a synchrotron and a dust component for the data sets A, B and C respectively (see text for details). The residuals for the Archeops data are traced in red on the figure. Notice that the millimetric data were not used in the fit. We show for each plot the full data set in the region of interest.

From left to right the plots on the top panel of figure 4 represent data sets A, B and C respectively as black data samples. The global best-fit model to the data is represented in red. The canonical synchrotron component is shown on light blue and the canonical dust in orange. The extra low temperature dust component is represented in blue. The parameters and error bars for the best-fit model to the data and the percentage of flux at 545 GHz associated to the extra component with respect to the total flux are given in table 3. We also present the χ^2/N_{dof} values for the global fit in the frequency range from 1 to 10^6 GHz and on the millimetric range from 100 to 1000 GHz.

For the three data sets we obtain a good global fit to the data as shown by the χ^2/N_{dof} values. The best-fit parameters obtained for the canonical synchrotron and dust components are in good agreement with those presented in Sect. 2. Comparing with Strom & Greidanus (1992), we found the same dust temperature, 46 ± 1 K, with an error bar improved by a factor of three, as we carefully account for the canonical synchrotron spectrum. For the data set A the amplitude of the extra component is compatible with zero and therefore we conclude that there are no evidence for an extra component in the form of low–temperature dust. For data sets B and C an extra component not compatible with zero at 95 % CL is favored. However, we observe that on the one hand the data require extremely low temperatures of 5 and 6 K, therefore dust masses of ∼230 and ∼ 110 $M_\odot$ for data sets B and C respectively, making the model rather unrealistic. On the other hand, the improvement of the χ^2/N_{dof} in the millimetric region between 100 and 1000 GHz is not significant to justify the addition of the three extra parameters required by the low-temperature dust component. This is also clear on the bottom panel of figure 4 where we represent from left to right the residuals to the best-fit model to the data on the millimetric regime for data sets A, B and C, respectively.

3.2. Extra synchrotron component

For the extra synchrotron component we consider, as in Bandiera *et al.* (2002), that the distribution of energy of the relativistic electrons responsible for the emission is well represented by a power law with spectral index in the range 1 to 3 and present a low-energy cutoff. To account for an excess of flux in the millimeter regime, the critical frequency corresponding to the lowest energy electrons must be somewhere in the range 200 to 600 GHz. In total the low-energy cutoff synchrotron model has three parameters, p the spectral index of the electron energy distribution, ν_c the low-energy cutoff critical frequency and A_{LECS}, a normalization coefficient. The best-fit to the data is found by χ^2 minimization.

For this case we have also performed our analysis on data sets A, B and C. The parameters and error bars of the best-fit to the data for the three data sets as well as the percentage of flux due to the extra component with respect to the total flux at 545 GHz are given on table 4. We also present χ^2/N_{dof} values for the best-fit to the data on the full data set from 1 to 10^6 GHz and on the millimetric regime from 100 to 1000 GHz. From left to right the plots on the top panel of figure 5 represents data sets A, B and C, respectively, as black data samples. The global best-fit model to the data is represented in red. The canonical synchrotron component is shown on light blue and the canonical dust in orange. The extra low-energy cutoff synchrotron component is represented in blue.

As above, for the three data sets we obtain a good global fit to the data as shown by the χ^2/N_{dof} values. The best-fit parameters obtained for the canonical synchrotron and dust components are in good agreement with those presented in Sect. 2 and on Strom & Greidanus (1992). For data sets A and C the amplitude of the extra synchrotron component is compatible with zero as well as the value of the spectral index of the electron energy distribution. We therefore conclude that

these two data sets show no evidence of an extra component in the form of low-energy cutoff synchrotron. For data set B the raw result is that the amplitude of the synchrotron component is non-zero at the 95% CL. However, the best-fit values for the spectral index p and the critical frequency ν_c are compatible with zero indicating that this component is not physical. In addition, we observe that for this data set the χ^2/N_{dof} in the millimetric region from 100 to 1000 GHz is worse than the one obtained in Sect 2.3 assuming the canonical model only. The bottom panel of figure 4 represents from left to right the residuals to the best-fit model to the data on the millimetric regime for data sets A, B and C, respectively. From these we conclude that the fit to the data in this regime is not improved by adding an extra synchrotron component.

We have also performed the analysis of the three data sets considering the p and ν_c parameters fixed and set to the values quoted by Bandiera *et al.* (2002). The analysis for the three data sets show that the amplitude of the extra synchrotron component is compatible with zero and therefore we conclude that the data show no evidence of millimetric excess.

4. Summary and conclusions

We present in this paper a comprehensive analysis of the SED of the Crab Nebula in the frequency range from 1 to 10^6 GHz. For this purpose we have used new data from the WMAP satellite (Page *et al.* 2006) and from the Archeops balloon experiment (Desert *et al.* (2008)) in addition to data currently available. We are mainly interested in the millimetric regime from 100 to 1000 GHz where an excess of flux with respect to the canonical model has been claimed by Bandiera *et al.* (2002). This canonical model assumes a synchrotron component with SED well represented by a power law with different spectral index at low and high frequency, *plus* a dust component corresponding to a modified black body emission at a temperature of $\sim$ 46 K and spectral index 2.

We have first characterized the canonical model. The low and high frequency synchrotron component were modeled by a simple power law with two free parameters, amplitude and spectral index and the fading of the Crab Nebula emission was accounted for by assuming a fixed value of 0.162 % per year. At high frequency, the best-fit model is compatible with previous results. However, at low frequency, the best-fit model considering the full data sets is not compatible with the "canonical" spectral index value $\beta \simeq -0.299 \pm 0.009$ from Baars *et al.* (1977). By contrast, when we exclude WMAP data (Page *et al.* 2006), or considering them on their own, the canonical value is recovered. This can be explained either by inter-calibration errors of $\sim$ 8% or by an evolution of the synchrotron SED towards a harder spectrum or by a dramatic change of the fading with time. As we are interested only in a possible millimetric excess, we leave that question open, and consequently considered three different data sets (full data, WMAP only and excluding WMAP) in which we searched for a millimetric excess.

Beside the canonical synchrotron, the IRAS data of the Crab Nebula emission show a large excess in the infrared, well explained by a modified black-body with a temperature of $\sim$ 46 K (Strom & Greidanus (1992)). As we considered in our analysis the low and high frequency data, we obtained an accurate estimation of this temperature, $\sim$ 46 $\pm$ 1 K, with error bar improved by a factor of three with respect to Strom & Greidanus (1992).

Concerning the millimetric excess, we first observed that the data are compatible with the canonical model. To check if an extra component may improve significantly the fit to the data, we consider either an extra low-temperature dust emission or an extra low-energy cutoff synchrotron component, as in (Bandiera *et al.* (2002)). In both cases, we conclude that the current data on the un-polarised Crab Nebula emission present no evidence of a millimetric excess with respect to the canonical synchrotron and dust model.

From this analysis, we conclude that considering an extra synchrotron with a low energy cutoff, we can exclude at 95% (CL) an excess of flux of 48 Jy at 545 GHz with respect to the canonical synchrotron. This is of importance for the calibration of the Planck satellite mission which will use the Crab Nebula for polarization cross-checks in the range 30 to 857 GHz.

Acknowledgements. We thank the Archeops collaboration for their efforts throughout the long campaigns. We acknowledge R. Bandiera for very helpful discussions. We finally thank Claudine Tur (LPSC) for fruitful help on bibliographic searches.

References

Aller H. D. & Reynolds S. P., 1985, Astrophys. J., 293, L73
Allen R. J.& Barrett A. H., 1967, Astrophys. J., 149, 1
Baars J. W. M., Hartsuijker A. P. , 1972, A&A, 17, 172
Baars J. W. M. *et al.*, 1977, A&A, 61, 99
Bandiera R. *et al.*, 2002, A&A, 386, 1044
Becklin E. E. & Kleinmann D. E., 1968, Astrophys. J., 152, L25
Chini R. *et al.*, 1984, A&A, 137, 117-127
Dmitrenko T. *et al.*, 1970, Radiofizika, Vol. 13, No. 6, 823-829
Desert F.-X., Macías-Pérez J. F. , Mayet F. *et al.*, 2008, to appear in A&A, astro-ph/0801.4502
Grasdalen G. L., 1979, PACS, 91, 436
Green D.A., Tuffs R.J. & Popescu C.C., 2004, MNRAS, 355, 1315-1326
Hobbs R. W., Corbett H. H., Santini N. J., 1968, Astrophys. J., 152, 43
Janssen M. A., Golden L. M. and Welch W. J., 1974, A&A, 33, 373-377
Kalaghan P. M. and Wulfsberg K. N., 1967, Astronomical J. , 72, 1051
Kellermann K. I., Pauliny-Toth I. I. K., Williams P. J. S., 1969, Astrophys. J., 157, 1
Kovalenko A. V., Pynzar' A. V., Udal'tsov V. A., 1994, Astronomy Reports, 38, 78-94
Macías-Pérez J. F. *et al.*, 2007, A&A, 467, 1313
Marsden P. L. *et al.*, 1984, Astrophys. J., 278, L29
Medd W. J., 1972, Astrophys. J., 171, 41
Mezger P. G. *et al.*, 1986, A&A, 167, 145
Penzias A. A. and Wilson R. W., 1965,Astrophys. J., 142, 1149
Page, L. *et al.*, 2006, Astrophys. J., submitted, astro-ph/0603450
Reynolds S. P., Chevalier R. A., 1984, Astrophys. J., 278, 630
Strom R. G. & Greidanus H., 1992, Nature, 358, 654
Véron-Cetty M. P. & Woltjer L., 1993, A&A, 270, 370
Vinogradova L. V. *et al.*, 1971, Radiofizika, Vol. 14, No. 1, 157-159
Vinyajkin E. N., 2005, astro-ph/0502033
Werner M. W. *et al.*, 1977, PACS, 89, 127
Wright E. L. *et al.*, 1979, Nature, 279,703
Wrixon G. T. *et al.*, 1972, Astrophys. J., 174, 399
Zabolotnyi V. F., Kostenko V. I., Slysh V. I. 1976, Soviet Astronomy, 19, 405

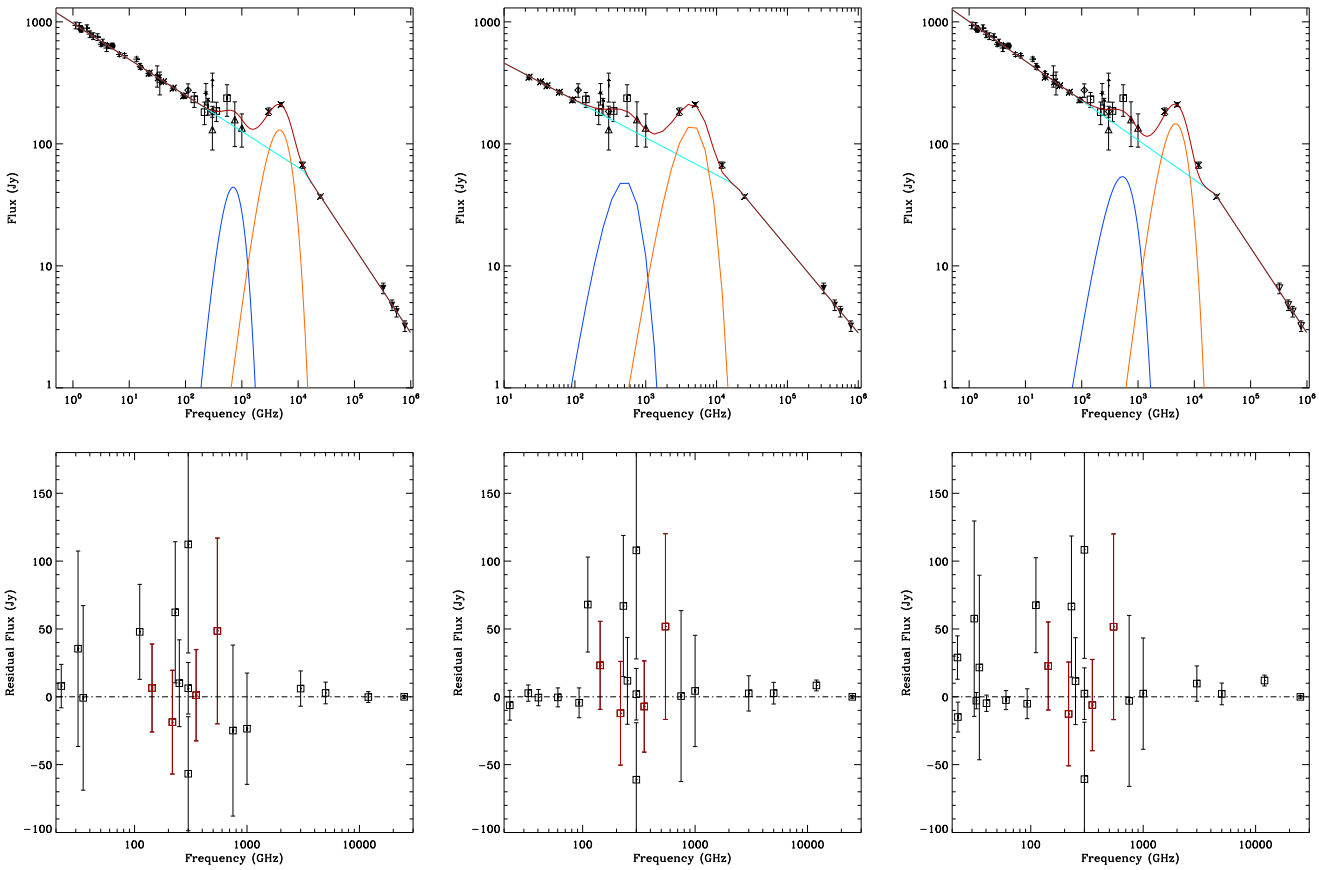

Fig. 4. Refined modelling of the SED of the Crab nebula in the frequency range from 1 to 10^6 GHz assuming an extra dust component at low-temperature. Top panel: from left to right the figures correspond data sets A, B and C respectively as discussed in the text. In black, red, light blue, yellow, and blue we represent the data, the best-fit model to the data and the synchrotron, the main dust and the extra dust components associated to it, respectively. Bottom panel: residuals in the millimetric regime for the top panel models. Notice that only the data used for the fit are represented in the figures.

Data Set	χ^2/N_{dof}	A_s (Jy)	A_D (Jy)	T_D (K)	β_D	A_{LTD} (Jy)	T_{LTD} (K)	β_{LTD}	LTD %	χ^2_{mm}/N_{dof}
A	0.68	973 ± 7	128 ± 7	45.9 ± 1.2	1.93 ± 0.50	31 ± 29	5 ± 17	3.7 ± 3.4	19 ± 18	0.97
B	0.59	927 ± 14	138 ± 8	45.9 ± 1	1.77 ± 0.29	49 ± 28	5 ± 8	1.8 ± 1.6	26 ± 15	1.20
C	0.90	1005 ± 10	144 ± 8	45.9 ± 1.6	1.89 ± 0.78	53 ± 32	6 ± 14	1.6 ± 1.3	29 ± 18	1.24

Table 3. Best-fit model parameters and errors for the extra dust component model for data sets A, B and C. χ^2/N_{dof} for the full data set and on the millimetric regime from 100 to 1000 GHz. Percentage of flux at 545 GHz due to the extra dust component with respect to the total flux.

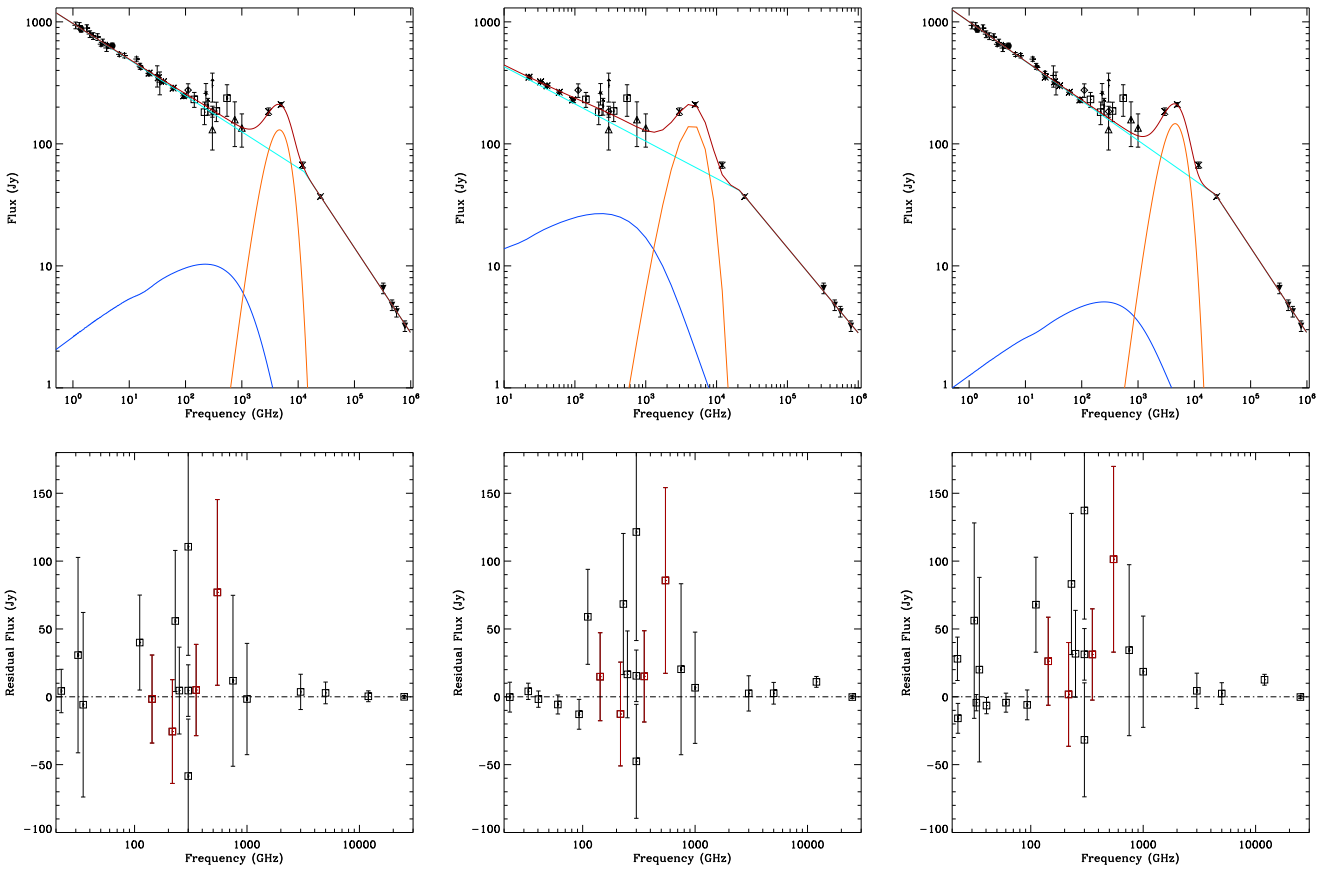

Fig. 5. Refined modelling of the SED of the Crab nebula in the frequency range from 1 to 10^6 GHz assuming an extra synchrotron component. Top panel: from left to right the figures correspond to the data sets A, B and C respectively as discussed in the text. In black, red, light blue, blue and yellow we represent the data, the best-fit model to the data and the main synchrotron, the extra synchrotron and the dust components associated to it, respectively. Bottom panel: residuals in the millimetric regime for the top panel models. Notice that only the data used for the fit are represented in the figures.

Data Set	χ^2/N_{dof}	A_s (Jy)	A_D (Jy)	T_D (K)	β_D	A_{LECS} (Jy)	ν_c (GHz)	p	LECS %	χ^2_{mm}/N_{dof}
A	0.67	966 ± 14	128 ± 9	45.9 ± 1.0	1.89 ± 0.4	9 ± 10	531 ± 298	5 ± 5	5 ± 6	0.91
B	0.72	868 ± 39	141 ± 8	45.9 ± 5.0	1.80 ± 0.4	24 ± 12	501 ± 1923	4 ± 14	15 ± 8	1.25
C	1.09	999 ± 12	143 ± 10	45.9 ± 1.0	1.80 ± 0.4	4 ± 6	459 ± 106	3 ± 10	3 ± 5	1.98

Table 4. Best-fit model parameters and errors for the extra syncrotron component model for data sets A, B and C. χ^2/N_{dof} for the full data set and on the millimetric regime from 100 to 1000 GHz. Percentage of flux at 545 GHz due to the extra synchrotron component with respect to the total flux.